

From semilocal density functionals to random phase approximation renormalized perturbation theory: A methodological assessment of structural phase transitions

Niladri Sengupta, Jefferson E. Bates,^{*} and Adrienn Ruzsinszky[†]
Department of Physics, Temple University, Philadelphia, Pennsylvania 19122, USA

 (Received 26 August 2017; revised manuscript received 20 December 2017; published 20 June 2018)

The structural phase transitions of different materials, including metal to metal, metal to semiconductor, and semiconductor to semiconductor transitions, were explored using methods based on the random phase approximation. Transition pressures for Si, Ge, SiC, GaAs, SiO₂, Pb, C, and BN from their stable low-pressure phases to certain high-pressure phases were computed with several semilocal density functionals and from the adiabatic connection fluctuation-dissipation formulation of density functional theory at zero temperature. In addition to the random phase approximation (RPA), three approximate beyond-RPA methods were also investigated to determine the impact of exchange-correlation kernel corrections. Results at finite temperature were obtained with the inclusion of zero-point energy contributions from the phonon spectra. We find that including temperature effects is most important for systems with nearly degenerate phases such as for boron nitride and carbon. In combination with thermal corrections, the kernel-corrected correlation methods deliver high accuracy compared to experimental data and can serve as a useful benchmark method in place of more expensive correlated calculations.

DOI: [10.1103/PhysRevB.97.235136](https://doi.org/10.1103/PhysRevB.97.235136)

I. INTRODUCTION

Structural phase transitions in solids are fascinating phenomena that have a large theoretical and practical importance. Space-group symmetry and associated internal structural parameters change from one crystal structure to another with the external influence of, for example, temperature or pressure. Temperature or pressure induced structural phase transitions can change the electronic structures of the corresponding materials, such as from insulator to metal and vice versa, or they may change the band structures of the insulating or metallic state resulting in a change in band gap or conductance. Structural phase transitions also sometimes lead to different magnetic states (e.g., antiferromagnetic to paramagnetic) [1]. Hence control of structural phase transitions presents many potential applications in electronics, optics, and other relevant fields [2–4]. Since it is challenging to experimentally determine coexistence temperatures or pressures of two different structural phases of a solid, a robust theoretical method is needed.

In order to predict accurate transition pressures for structural phase transitions in solids, accurate equilibrium geometries and energy differences between the respective phases are required. Density functional approximations such as from the local density approximation (LDA) and generalized gradient approximations (GGAs) yield reasonably accurate structures [5], but tend to underestimate the energy difference between low and high pressure phases [6,7]. One of the most fundamental aspects of density functional theory is self-interaction error (SIE) [8], also known as the delocalization error. Hartree-Fock (HF) is a one-electron, self-interaction error free method by

construction, and like the HF method, exact density functional theory would also be SIE free. However, for practical approximate density functionals some part of the SIE remains [9]. This leads to a considerable reduction of the accuracy for the description of a variety of physical processes [10]. Systems with *d* or *f* electrons containing both localized orbitals and delocalized orbitals are genuinely plagued by the SIE [11]. A natural solution to these challenges, the adiabatic connection fluctuation-dissipation (ACFD) formulation of density functional theory (DFT) is constructed from a self-interaction free exchange energy and a nonlocal correlation energy that directly accounts for dispersion [12–14]. The random phase approximation (RPA) is the simplest approximation within ACFD-DFT and has proven to be a highly accurate method for treating weak interactions [15–19] and predicting structural properties [20–24] and energetics [25,26]. Although RPA captures intermediate- and long-range correlations, it does not accurately account for short-range correlation [27–30]. RPA was previously used to study the pressure-induced phase transitions of Si and SiO₂, delivering an improvement over semilocal functionals for Si, but yielding mediocre results for SiO₂ likely due to an imperfect cancellation of errors [7]. To go beyond RPA, a kernel correction from time-dependent DFT or many-body perturbation theory must be included to correct the short-ranged behavior of RPA and improve the systematic performance of ACFD-based methods [31–35]. To study the improvements ACFD methods may bring compared to semilocal functionals, we have investigated the pressure-induced phase transition of several materials.

The diamond structures of silicon and germanium are indirect band gap semiconductors, and at high pressures their properties are remarkably similar though not identical. The semiconducting diamond phases of both materials undergo a transition to the metallic beta-tin (β -Sn) phase under pressures

^{*}jeb@temple.edu

[†]aruzsinszky@temple.edu

in the range of 10–14 GPa [6]. Beta-tin was predicted to be the most favored structure of Si and Ge at high pressures among several other possibilities by first-principles calculations in agreement with experiment [36]. The relative stability of the cubic diamond and beta-tin phases of Si and Ge has been the subject of previous theoretical studies and has become a benchmark for several theoretical methods [37,38]. Still, more accurate theoretical methods would be welcome to resolve the discrepancies between Monte Carlo and density functional calculations [7].

Silicon carbide (SiC) is an indirect band gap semiconductor and crystallizes in the zinc blende (ZnS) structure under normal conditions. Due to its stability over a wide range of temperatures and pressures, it has been used in high-power electronics and in integrated circuits as a reliable base to support other materials [39]. It is also frequently used in composite materials and related applications as a hard ceramic material [40]. Theoretical studies first showed that among several possible high-pressure structures, rocksalt is the most energetically stable for SiC [41,42]. The rocksalt phase is also metallic, in contrast to the low-pressure phase. Yoshida *et al.* later reported an experimental structural phase transition from zinc blende to metallic rocksalt at 100 GPa [43]. Further theoretical studies have confirmed these earlier works, but theoretical values largely underestimate the experimental transition pressure [44–46] most likely due to a thermodynamic barrier that must be overcome in the experiment [47], but not in the calculations [45].

Gallium arsenide (GaAs) is a wide band gap semiconductor and crystallizes in the zinc blende (ZnS) structure under normal conditions. Due to its higher electron mobility and higher saturated electron velocity it is suitable to operate at high frequencies [48,49]. Due to its direct band gap, GaAs shows strong photoemission as well [50,51]. These properties, coupled with a high dielectric constant, are the reasons GaAs is widely used in integrated circuits, interstellar electronics, optics, and solar cells [49,52–55]. Minomura and Drickamer observed a pressure-induced phase transition in GaAs [56] at 24 GPa by high-pressure electrical resistance experiments. Afterwards, many theoretical and experimental studies confirmed that GaAs undergoes a structural phase transition from the semiconducting zinc blende structure to a metallic state with orthorhombic symmetry at 17 GPa under compression [6,57]. Finally McMahon *et al.* correctly identified the structure of that metallic phase as the site-ordered *Cmcm* structure [58]. Besson *et al.* also extensively studied forward and reverse transitions experimentally between low-pressure and high-pressure phases using optical-transmittance measurements, Raman scattering, and x-ray absorption techniques, suggesting the thermodynamic transition pressure of ZnS to the *Cmcm* phase of GaAs at about 13.5 GPa around 300 K [59].

Silica (SiO₂) is used in a variety of applications such as in the production of glass or in optical fibers for telecommunications [60]. Previous theoretical studies have reported structural parameters, elastic constants, and bulk moduli of different phases of silica, including quartz and stishovite phases, using LDA and GGA functionals [61–63]. Consistent with those previous works, Xiao *et al.* [7] also reported the pressure-induced phase transition of silica from the low-pressure quartz phase to the high-pressure stishovite phase at around 7 GPa,

which is accompanied by a change in coordination of the Si atoms and subsequently a large increase in the hardness of the material. Xiao *et al.* [7] demonstrated that most semilocal functionals struggle to predict accurate structural parameters or phase transition parameters, with the exception of the PBE [64] GGA and a certain class of meta-GGAs [65]. Though RPA predicts accurate structural properties for the two materials, it underestimates the energy difference between the phases resulting in an underestimation of the transition pressure [7]. The authors of Ref. [7] suggest that this apparent failure of RPA is likely due to an imperfect cancellation of errors, and we further support this assessment below by demonstrating the impact of an exchange-correlation kernel on the computed transition pressure and energy difference between phases.

Pb is a metal and crystallizes in the fcc structure under normal conditions, but a transition to the hcp structure is observed at 14 GPa [66,67]. The volume reduction is very small at the transition and therefore there is a large region of phase coexistence, consistent with a very small enthalpy difference between the phases over a large pressure interval. Liu *et al.* [68] studied the stability of Pb at high pressures using plane wave pseudopotential methods, including scalar-relativistic and spin-orbit effects. The three structural phases fcc, hcp, and bcc were found to be very close in energy, but nonetheless the sequence of transitions was correctly described, as well as the structural properties of the phases. Hermann *et al.* also studied Pb with and without relativistic effects and found that the structural properties of the hcp are much more strongly affected than those of the fcc phase [69].

Diamond and cubic boron nitride are similar materials; both of them are extremely hard and have very high melting points [70]. They are mostly chemically inert and have a large thermal conductivity [70]. Cubic BN (c-BN) does not dissolve in iron and steel and thus is an excellent material for the protective coating of heavy tools [70]. It has a wide band gap and relatively small dielectric constant, so it has great applications in the domain of UV optics and high-temperature microelectronics [70,71]. DFT and experimental studies indicate that the diamond-like c-BN is more stable than the graphite-like hexagonal (h-BN) [72–74]. Due to the heteropolarity effect, the equilibrium energy difference of the cubic and hexagonal phases of BN is much larger than those found between the diamond and graphite phases in carbon [6]. Even including the effects of zero-point energy and the finite temperature using the quasiharmonic approach, Albe *et al.* [75] and Kern *et al.* [76] did not find very accurate transition pressure compared to the experiment.

The diamond and graphite phases of carbon are very different from each other, unlike BN. Diamond is an indirect, wide band gap insulator while graphite is a layered, zero band gap semimetal. Diamond has a large thermal conductivity and is mostly chemically inert like cubic BN. Diamond is also a very hard material owing to its strong sp^3 hybridization [6]. Graphite, however, is a soft and stiff material with very high thermal stability and high thermal and electrical conductivity due to the inability of phonons to propagate quickly between layers with weak interaction and the availability of delocalized free electrons between the layers, respectively [6]. Experiments have confirmed that graphite is the stable phase under normal conditions and that it can undergo a phase transition to the

diamond phase around 1.7 GPa at 0 K and around 12 GPa at 5000 K [77]. Also the energy difference between graphite and diamond is very small, around 5–20 meV at 0 K [78]. Most of the semilocal functionals either yield the wrong ordering of the phases with respect to experiment or overestimate the energy difference [73,79]. Even RPA cannot provide correct ordering of the phases and energy difference since it shows those phases are essentially degenerate at 0 K [78].

Recently, Cui *et al.* showed that the relative stability of TiO₂ in the rutile and anatase structure is correctly described by RPA. They further concluded that including the zero-point energy and finite-temperature effects based on the harmonic approximation increases the relative stability of the rutile phase compared to the anatase phase, and leads to a better quantitative agreement with experimental measurements [80]. Whittleton *et al.* also found that thermal corrections are very important for accurate energy ranking of the polymorphs of organic molecular crystals [81]. In their work, 4-hydroxythiophene-2-carbonitrile’s experimental structure is only correctly identified once a quasiharmonic estimate of the vibrational free-energy contribution is included. Our results also show that when the energy difference between phases for bulk solids is close to zero, the temperature corrections are crucial for determining the most stable phase.

In the following we briefly describe the applied methods in Sec. II and the computational details in Sec. III, and we present the results for each system in Sec. IV. A brief discussion and conclusions are then given in Sec. V.

II. METHODS

In order to apply density functional theory to real systems, an approximation for the unknown exchange-correlation (xc) energy is needed. Within the hierarchy of approximate functionals [82], approximations such as the local density approximation [83] (LDA) depend only on the electron density. Higher-level functionals, such as GGAs or meta-GGAs, incorporate gradients of the density and dependence on the kinetic-energy density, respectively. The accuracy of nonempirical functionals tends to be connected to their satisfaction of exact constraints on the xc energy, culminating in the development of the strongly constrained and appropriately normed (SCAN) meta-GGA which satisfies all the possible constraints that a meta-GGA can [84]. Through its dependence on the kinetic energy density, SCAN is able to capture intermediate-range van der Waals interactions, but is lacking long-range weak interactions [85,86]. In this work we will utilize the GGA of Perdew, Burke, and Ernzerhof (PBE) [64], in addition to LDA and SCAN, as representative examples of semilocal density functionals in order to compare their performance to the results from the adiabatic connection. Since these semilocal functionals still contain self-interaction errors [8,9], we can investigate how including long-range dispersion in spite of SIE in these approximate methods influences the results compared to methods that are SIE free and contain long-range dispersion effects, such as RPA.

In order to incorporate long-range dispersion, methods such as Vydrov and van Voorhis’s VV10 and revised VV10 (rVV10) were developed to provide the missing dispersion by adding a nonlocal correlation component to semilocal exchange-

correlation energy such that $E_{xc} = E_{xc}^0 + E_c^{nl}$, where E_{xc} is the total exchange correlation energy [87,88]. Both the original VV10 and rVV10 have the flexibility to be tuned to different semilocal functionals [19], though we will only explore their combination with SCAN and PBE, and take the relative results compared to the bare functional as indicative of the performance for any semilocal functional. We note, however, that the addition of rVV10 to SCAN does not contaminate the accurate intermediate-range vdW description of the bare SCAN functional [85]. Grimme’s empirical dispersion correction scheme was also explored in both the D2 [89] and D3 [90,91] variants, in order to make comparisons with the nonlocal rVV10 correction. To go beyond the lowest three levels of approximation within DFT and naturally include long-range vdW interactions, we utilized “fifth-rung” methods from the ACFD-DFT formalism.

The total energy within the ACFD-DFT formalism is obtained from the sum of a self-interaction error free exchange energy and the correlation energy,

$$E^{\text{ACFD}} = E^{\text{EXX}} + E_c^{\text{ACFD}}. \quad (1)$$

The exact exchange (EXX) energy is equivalent to the Hartree-Fock energy evaluated with DFT orbitals [13,14], while the correlation energy E_c can be obtained exactly from knowledge of the interacting density-density response function [92]. In practice, the interacting response function is obtained from approximate time dependent (TD) DFT either within RPA or through the inclusion of an approximate xc kernel, typically within the adiabatic approximation [93,94]. In this work we have explored both RPA and beyond-RPA (bRPA) methods to understand the importance of short-ranged correlation effects in predicting structural phase transitions. These methods also shed light on the balance of nonlocal exchange and correlation, and the fortuitous error cancellation exhibited by semilocal functionals. Since PBE reference orbitals are typically used to evaluate RPA, we have elected to use the spatially renormalized, adiabatic PBE exchange-like kernel [35] (rAPBE) to evaluate the bRPA contribution to the correlation energy.

We should also be clear that the arbitrary use of PBE orbitals to evaluate the response functions and kernels is itself an approximation, whenever the kernel used to determine the response function is not derived from the second functional derivative of the PBE xc energy [33,35,94]. Previous works have shown this dependence to be fairly weak among semilocal functionals for energy differences and structural properties [16,20,33–35,95], so we assume it extends to the calculations herein as well.

In order to efficiently treat the bRPA correlation energy we utilize three approximations from RPA renormalized (RPAr) perturbation theory [30,34,96]: first-order RPA renormalization (RPAr1), a higher-order terms (HOT) correction beyond RPAr1 [97], and the ACSOSEX approximation [32]. The essence of RPAr is that the total correlation energy can be exactly decomposed as

$$E_c^{\text{ACFD}} = E_c^{\text{RPA}} + \Delta E_c^{\text{bRPA}}, \quad (2)$$

and the different methods mentioned above involve different approximations for ΔE_c^{bRPA} . RPAr offers a modest speedup compared to the traditional bRPA approach [98] with little

loss in accuracy [30,96,99]. The main difference between each bRPA method lies in the treatment of third- and higher-order contributions to the many-body perturbation theory expansion of the correlation energy, though all three methods yield the exact second-order contribution if used with the exact kernel [30]. Since all three methods require the computation of the RPA response function and the exchange-correlation kernel, they can be evaluated simultaneously with the RPA correlation energy once the kernel has been computed [96].

RPAr1 has been previously used in tandem with an approximate exchange kernel [34], the frequency-dependent exact exchange kernel [99], and several approximate kernels from TDDFT [96], delivering high-accuracy without worry of electronic instabilities in the response function [34,99,100]. Though several approximate kernels are available, the use of an exchange-like kernel should provide a general picture of the behavior of kernel corrections while keeping the computational cost close to RPA. Furthermore, advanced exchange-correlation kernels (nonlinear in λ) did not yield significant differences compared to exchange-like kernels for structural properties of simple solids [24], though the discrepancies for energy differences is still an open question.

III. COMPUTATIONAL DETAILS

The calculations were performed using a modified version of GPAW [101,102], a Python-based software built on the Atomic Simulation Environment (ASE) package [103] and utilizing the projector augmented wave (PAW) method [104]. GPAW was used to compute the PBE [64] results discussed below, and PBE orbitals were used as input for the ACFD methods since they are evaluated non-self-consistently. Gamma-centered Monkhorst-Pack [105] k meshes were used throughout. For the beyond-RPA calculations the rAPBE kernel [35] was used with wave vector symmetrization [24,106] throughout. Results from the strongly constrained and appropriately normed (SCAN) meta-GGA were obtained with the

VASP [107] software package using PBE PAWs that include the kinetic energy density component for B, N, Si, O, and C and normal PBE PAWs that include the fully occupied d -shell electrons as well as the kinetic energy density component for Ga, As, Pb, and Ge. We have carefully done convergence tests for each material with PBE, exact exchange (EXX), and the RPA correlation energy contribution with regards to the cutoff energy of the input wave functions and the k mesh. All parameters were chosen to yield errors on the order of 0.02 eV per functional unit or less. The converged parameters we used are reported in the Supplemental Material [108]. EXX tends to be more difficult to converge, and typically requires larger cutoffs compared to semilocal functionals.

From the phonon spectrum, the zero-point energy contribution and finite-temperature corrections can be obtained to study temperature-dependent transition pressures. We have calculated the phonon spectra from first-principles calculations based on DFT as implemented in VASP [107]. Density functional perturbation theory [109,110] has been used to compute the dynamical matrices for all materials. Then we used our own code to calculate the temperature-dependent phonon entropy contribution from the above data. We used the same cutoffs, k meshes, and PAWs [111] for the phonon calculations as for our zero-temperature energy calculations. Previous studies have shown that different density functionals produce similar results for the zero-point energy [112] (ZPE) and thermal corrections to the transition pressure [7]; hence we have used only PBE to compute the phonons. In some special cases at high temperature (>4000 K) and pressure (>150 GPa), anharmonic effects play a crucial role and using the same functional for electronic and vibrational calculations is important for a proper prediction of thermodynamic properties [113–115]. The interplay of approximations for the van der Waals forces and the ground state functional can also be important when considering which methods to use at high temperatures [116]. For our room temperature calculations, however, the effect on the thermodynamic parameters when choosing a different

TABLE I. Equilibrium cell volumes (\AA^3) obtained from the EOS fits for each method. SCAN tends to be the most accurate semilocal functional, while the ACFD methods tend to overestimate by as much as LDA underestimates.

Materials	LDA	PBE	SCAN	EXX	RPA	RPAr1	HOT	ACSOSEX	Expt. ^a
Si (Diamond)	39.503	41.048	39.976	41.348	40.460	40.744	40.663	40.507	40.037
Si (Beta-tin)	59.540	61.583	59.772	63.652	61.489	61.082	60.793	60.447	55.820 [133]
Ge (Diamond)	44.644	47.942	45.287	44.966	46.073	46.368	46.314	46.102	45.271
Ge (Beta-tin)	71.655	77.030	74.214	76.133	75.037	74.908	74.617	74.169	
SiC (ZnS)	20.408	21.148	20.607	20.759	21.003	20.993	20.944	20.817	20.693
SiC (Rocksalt)	16.260	16.868	16.342	15.757	16.599	16.565	16.521	16.403	16.554 [44]
GaAs (ZnS)	44.684	48.028	45.592	45.448	46.854	47.097	47.073	46.923	45.138
GaAs (<i>Cmcm</i>)	143.509	154.249	147.248	151.868	154.077	152.393	151.640	150.435	
SiO ₂ (Quartz)	36.822	40.351	37.357	40.881	37.939	38.478	38.528	38.594	37.803
SiO ₂ (Stishovite)	23.351	24.445	23.284	22.799	23.896	23.922	23.895	23.711	23.325
Pb (fcc)	28.908	31.815	30.648	34.190	29.726	30.556	30.535	30.471	30.010
Pb (hcp)	57.468	63.326	60.976	68.916	59.250	60.929	60.875	60.686	48.530
C (Diamond)	11.024	11.403	11.240	11.132	11.373	11.336	11.312	11.228	11.345
C (Graphite)	34.548	35.599	34.935	34.381	35.436	35.618	35.227	34.966	36.615
BN (Cubic)	11.482	11.915	11.742	11.563	11.780	11.764	11.744	11.660	11.664
BN (Hexagonal)	35.500	36.683	35.963	35.478	36.266	36.387	36.367	36.110	36.701

^aExperimental reference values were taken from the reported ICSD values via the Materials Project database [134] unless otherwise specified.

functional for the phonon calculations is not significant. This is in line with some previous authors' results [7,112]. To compare with existing literature equilibrium cell volumes, the results in the Table I do not include the shifts due to the phonon corrections [7].

The Gibbs free energy is $G(V,T) = E(V,T) - TS(V,T) + P(V,T)V = F(V,T) + P(V,T)V$, where $E(V,T)$ is the internal energy and $F(V,T) = E(V,T) - TS(V,T)$ is the Helmholtz energy. At the transition pressure, the difference in Gibbs free energies for the two phases should be equal to zero. Moreover, at zero temperature, the Gibbs free energy reduces to the enthalpy, $H(V) = E(V) + P(V)V$, and so the transition pressure is the pressure where the enthalpy difference between phases is equal to zero. $E(V)$ and $P(V)$ can also be denoted as $E(V, T=0)$ and $P(V, T=0)$, emphasizing that they are zero-temperature energy and pressure.

Structural parameters for each phase, such as the equilibrium cell volume (V_0) and corresponding equilibrium energy (E_0), bulk modulus (B_0), and pressure derivative of the bulk modulus (B'_0), can be evaluated by fitting the energy-volume (E - V) data generated through density functional theory to the standard third-order Birch-Murnaghan (BM) equation of state [117,118] (EOS) given by

$$E(V) = E_0 + \frac{9B_0V_0}{16} \left\{ \left[\left(\frac{V_0}{V} \right)^{2/3} - 1 \right]^3 B'_0 + \left[\left(\frac{V_0}{V} \right)^{2/3} - 1 \right]^2 \left[6 - 4 \left(\frac{V_0}{V} \right)^{2/3} \right] \right\}. \quad (3)$$

The pressure can also then be computed analytically as $P(V) = -\left(\frac{\partial E(V)}{\partial V}\right)$, after determining the four fitting parameters (E_0, B_0, V_0, B'_0) from Eq. (3),

$$P(V) = \frac{3B_0}{2} \left[\left(\frac{V_0}{V} \right)^{7/3} - \left(\frac{V_0}{V} \right)^{5/3} \right] \times \left\{ 1 + \frac{3}{4}(B'_0 - 4) \left[\left(\frac{V_0}{V} \right)^{2/3} - 1 \right] \right\}. \quad (4)$$

The transition pressures and volumes are determined by a brute force numerical minimization of the enthalpy or Gibbs free energy difference between phases at zero and finite temperature, respectively. We compute the enthalpies of the respective phases at their corresponding equilibrium volumes with the help of Eq. (3) and Eq. (4). Starting from a guess for the transition pressure, $P_{t,0} = 0.5 \frac{\Delta E_0}{\Delta V_0}$, the pressure is iteratively increased or decreased to force the enthalpy difference between phases to zero. We use a convergence threshold of at least 10^{-4} eV per atom to ensure tight convergence of the phase transition parameters. We have provided our code for this procedure as a part of the Supplemental Material [108].

To include the zero-point motion and thermodynamic contributions from vibrational degrees of freedom, we use the Helmholtz free energy. For a lattice, the Helmholtz free energy is given within the quasiharmonic approximation [119–122]

(QHA) as

$$\begin{aligned} F(V,T) &= E(V,T) - TS(V,T) \\ &= E(V) + \sum_{q,j} \frac{\hbar\omega_{q,j}(V)}{2} \\ &\quad + k_B T \sum_{q,j} \ln \left[1 - \exp \left(-\frac{\hbar\omega_{q,j}(V)}{k_B T} \right) \right] \\ &= E(V) + k_B T \sum_{q,j} \ln \left[2 \sinh \left(\frac{\hbar\omega_{q,j}(V)}{2k_B T} \right) \right], \quad (5) \end{aligned}$$

where $E(V,T)$ is the lattice crystal energy at a specified volume and temperature, and $\omega_{q,j}(V)$ is a computed phonon frequency.

At a finite temperature, the Gibbs free energy, $G(V,T) = F(V,T) + V P(V,T)$, should be obtained from $F(V,T)$ and

$$P(V,T) = -\left(\frac{\partial F}{\partial V}\right)_T. \quad (6)$$

For that purpose, we have done the EOS fitting of $F(V,T)$ from Eq. (5) to an isothermal third-order BM EOS,

$$\begin{aligned} F(V,T) &= F_{0T} + \frac{9B_{0T}V_{0T}}{16} \left[\left(\frac{V_{0T}}{V} \right)^{2/3} - 1 \right]^3 B'_{0T} \\ &\quad + \left[\left(\frac{V_{0T}}{V} \right)^{2/3} - 1 \right]^2 \left[6 - 4 \left(\frac{V_{0T}}{V} \right)^{2/3} \right], \quad (7) \end{aligned} \quad (8)$$

where F_{0T} is the Helmholtz free energy at the equilibrium volume, and each of the fitting parameters ($F_{0T}, B_{0T}, V_{0T}, B'_{0T}$) depends implicitly on temperature (indicated by the subscript) due to the phonon correction. Analogously, the pressure is then obtained from Eq. (9) using the isothermal EOS fitting parameters

$$\begin{aligned} P(V,T) &= -\left(\frac{\partial F}{\partial V}\right)_T \\ &= \frac{3B_{0T}}{2} \left[\left(\frac{V_{0T}}{V} \right)^{7/3} - \left(\frac{V_{0T}}{V} \right)^{5/3} \right] \\ &\quad \times \left\{ 1 + \frac{3}{4}(B'_{0T} - 4) \left[\left(\frac{V_{0T}}{V} \right)^{2/3} - 1 \right] \right\}. \quad (9) \end{aligned}$$

After that, the same numerical procedure is then used to obtain the phase transition pressure as for the zero-temperature case [123].

In principle the approximation used to compute E_{xc} for the electronic energy should also be used to compute the phonon spectra. However, this is not possible for many meta-GGA and ACFD functionals, because analytic second derivatives of the potential energy with respect to nuclear positions have not been implemented in any code, and performing finite differences would be too expensive for the latter methods. In fact, only recently were the first derivatives for RPA implemented for periodic systems [124]. Since we use PBE input orbitals for the ACFD methods, and SCAN phonons are unavailable, we have elected to use the phonon spectra predicted by PBE to compute all of the thermal effects in our work. It was confirmed that this was a reasonable approach for BN, GaAs, and Si, by computing

the LDA phonon spectra and adding LDA thermal effects; the resulting transition pressures were negligibly different from the reported results herein using the PBE phonon spectra. The Birch-Murnaghan EOS is not the only choice for fitting E - V data, and several other equations of state have been used in the literature to compute thermodynamic properties from DFT calculations [46,125–132].

IV. RESULTS

It is well known that LDA and PBE tend to underestimate and overestimate structural parameters of molecules and materials [5,127,135], while SCAN was recently demonstrated to improve upon both of these methods for energetics and structures [136]. Our results for the materials studied herein reflect these same trends, with SCAN being the most accurate semilocal functional for predicting the equilibrium structural parameters; see Table I and Fig. 1. For the ACFD methods, EXX overestimates the lattice constants as often as it underestimates due to neglect of correlation, but on average is only slightly worse than PBE itself. The addition of correlation from RPA or bRPA methods typically improves the agreement with experiment, though the structural parameters tend to be overestimates. Comparing all methods, SCAN is the most accurate for predicting structural properties, while PBE is the worst. On average, LDA underestimates the equilibrium volume by roughly the same amount that RPA and bRPA methods overestimate it. Consequently, the performance for the transition pressure shows similar trends among semilocal and ACFD methods, though there are some differences for comparing performance across all methods. We note that our SCAN results for several materials are in good agreement with those of Ref. [137], though a ~ 4 GPa discrepancy for Pb was discovered due to slightly different procedures used to obtain the EOS fit for the hcp phase.

To compare the various electronic structure methods we can divide the materials into the three broad groups based on their phase transitions. First is the phase transition between

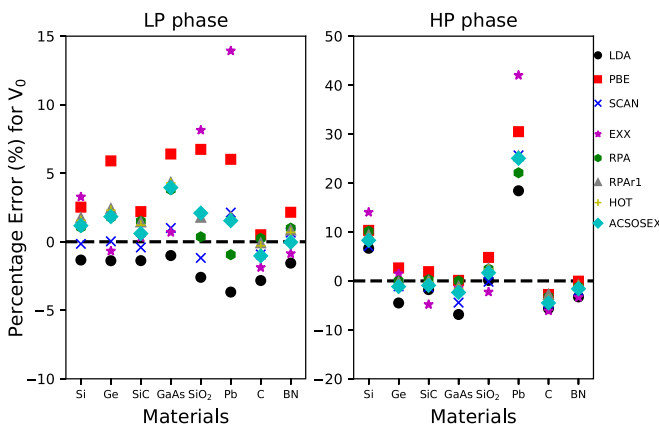


FIG. 1. Percentage error of the equilibrium volume (V_0) of different materials for high-pressure (HP phase) and low-pressure (LP phase) phases relative to the reference for different methods. Either experiment or RPA was used as a reference. Negative and positive values represent underestimation and overestimation of V_0 compared to the corresponding reference value, respectively.

TABLE II. Transition pressures (GPa) without temperature corrections.

Materials	LDA	PBE	SCAN	EXX	RPA	RPAr1	HOT	ACSOSEX
Si	7.3	9.7	14.5	51.4	13.8	11.4	10.7	11.1
Ge	6.5	8.1	11.3	51.1	11.2	10.4	10.1	10.9
SiC	61.0	65.8	74.1	114.6	74.3	71.4	70.3	71.0
GaAs	10.5	12.8	17.1	60.2	18.9	17.2	17.0	17.5
SiO ₂	-0.7	5.8	4.6	12.8	3.7	6.6	6.9	6.8
Pb	11.1	13.6	16.4	31.3	19.0	16.7	16.5	16.1
C	-0.6	6.1	4.6	7.8	0.6	6.7	6.7	6.8
BN	-3.3	3.2	2.8	10.8	-1.5	0.9	1.1	1.2

two highly symmetric phases such as in Si, Ge, and SiC. The second group concerns phase transitions between two dissimilar phases composed of at least one lower-symmetry phase such as in GaAs (low-symmetry phase: $cmcm$) and SiO₂ (low-symmetry phase: quartz). Lastly, there are the special cases, such as the metal to metal phase transition of Pb, and the phase transition between two nearly degenerate phases such as in C and BN.

A. Phase transitions between highly symmetric phases

Considering the first group of materials and semilocal functionals at zero temperature, Table II and Fig. 2 illustrate that SCAN overestimates the transition pressures of Si and Ge in comparison to experiment, while PBE and LDA underestimate them (experimental values are given in Table IV). Our results are in good agreement with previous studies using the latter two functionals [6,65]. Our SCAN results yield an energy difference between phases of 0.417 eV per functional unit for Si which is equivalent to what Sun *et al.* reported in their previous study of this system [136]; see Table III. For the ACFD methods, EXX evaluated with PBE orbitals yields a very large overestimate of the transition pressures that is directly linked to its large overestimate of the energy difference between phases in both materials. Adding correlation from RPA significantly reduces the errors of EXX and results in

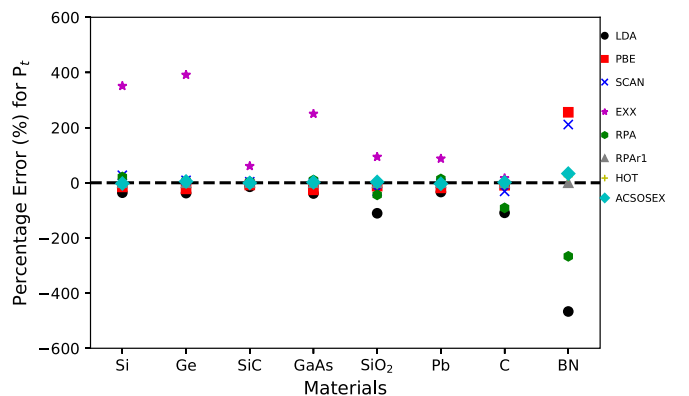


FIG. 2. Percentage error of the predicted transition pressure (P_t) at zero temperature for different materials with respect to the reference values. RPAr1 was used as a reference. Negative and positive values represent underestimation and overestimation of the transition pressure compared to the corresponding reference value, respectively.

TABLE III. Equilibrium energy differences without temperature corrections, reported in eV/functional unit.

Materials	LDA	PBE	SCAN	EXX	RPA	RPAr1	HOT	ACSOSEX
Si	0.212	0.289	0.417	1.260	0.384	0.334	0.317	0.328
SiC	1.348	1.471	1.631	2.662	1.655	1.606	1.583	1.599
Ge	0.168	0.220	0.265	1.046	0.276	0.267	0.262	0.280
GaAs	0.525	0.668	0.825	2.362	0.990	0.952	0.946	0.978
SiO ₂	-0.061	0.489	0.356	1.092	0.2488	0.508	0.535	0.542
Pb	0.010	0.012	0.015	0.041	0.035	0.027	0.026	0.027
C	-0.013	0.120	0.088	0.145	0.012	0.129	0.130	0.130
BN	-0.130	0.126	0.105	0.405	-0.057	0.038	0.044	0.048

only slight overestimates of the transition pressures, which are further reduced by the addition of bRPA correlation from rAPBE with any of the RPAr approximations. The bRPA results are consequently slight underestimates in comparison to experiment and the resulting errors are quite close to one another, and comparable to RPA but with the opposite sign. Figure 3 shows the comparison between RPA and the HOT approximation for Ge, demonstrating the similarity of these methods for these high-symmetry systems.

Comparing semilocal and ACFD methods, LDA and PBE are clearly inferior to the ACFD methods while SCAN's performance is quite close to RPA. The bRPA methods are the most accurate, even though there is some error in the equilibrium structural parameters. As discussed above, there is a remarkably large error for all methods in comparison to experiment for the transition pressure of SiC. Thus we find it more appropriate to compare electronic structure methods among themselves instead of to experiment since the computed values all correspond to the same thermodynamic process

and do not consider the impact of transition barriers on the transformation. We have seen for Si and Ge that the bRPA methods with the rAPBE kernel yield the most accurate results compared to the corresponding experiments, so we will use the RPAr1 value as a "reference" for SiC. We note that the choice of RPAr method makes little difference since they all lie within approximately 1 GPa of each other. In this way, the analysis for Si and Ge is completely transferrable to SiC and hence why we have grouped them together; SCAN yields a small overestimate of the transition pressure in SiC though it is close to RPA, LDA and PBE are clear underestimates, EXX is a drastic overestimate, and RPA greatly reduces the errors of EXX but still slightly overestimates compared to the bRPA methods.

With the addition of finite-temperature corrections from the computed phonon spectra of PBE, the transition pressures for Si, Ge, and SiC all shift to smaller values indicating a stability of the high-temperature phase in each case, Table IV. The shifts are fairly small here, and do not significantly change the relative trends among the functionals. SCAN and RPA are now closest to experiment for Si and Ge, and the bRPA methods yield slightly larger underestimates. For SiC, SCAN and RPA still remain close to one another and to the bRPA methods.

We have also tested the effect of adding different long-range dispersion corrections for silicon as a representative example of this group of materials. Numerical results are presented in the Supplemental Material [108]. We have found that the most recent iteration of Grimme's empirical dispersion correction scheme, DFTD3 [90,91], when parametrized for SCAN [86] yields similar shifts in the equilibrium volumes, energy difference between phases, and subsequently the transition pressures compared to previous calculations using PBE and DFTD2 [89]. The same is true for more advanced dispersion corrections

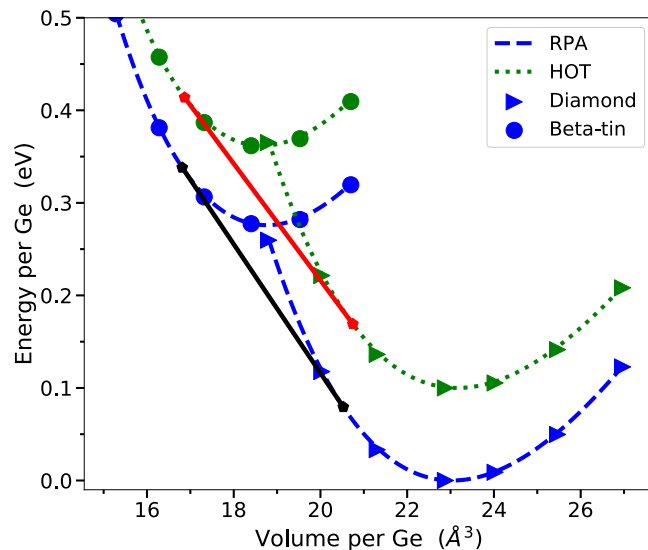


FIG. 3. E - V curve for diamond and beta-tin phases of Ge with RPA and bRPA per functional unit. The kernel corrections for Ge decrease slightly the equilibrium energy difference of the phases and hence slightly underestimate the transition pressure compared to RPA. The kernel-corrected curves have been rigidly shifted up in energy by 0.1 eV compared to RPA for visual clarity. The solid lines represent the common tangent between phases, the slope of which is equal to the negative of the predicted transition pressure.

TABLE IV. Transition pressures (GPa) including temperature corrections at room temperature, 300 K.

Materials	LDA	PBE	SCAN	RPA	RPAr1	HOT	Expt. [6]
Si	6.3	8.5	13.8	12.8	10.4	9.7	12.0
Ge	5.6	7.1	10.4	10.2	9.5	9.2	10.6
SiC	56.4	61.4	69.1	69.6	66.8	65.6	100.0
GaAs	9.4	11.6	16.1	18.0	16.3	16.0	15.0
SiO ₂ ^a	-0.1	6.4	5.2	4.3	7.1	7.4	7.5 [141]
Pb	17.8	21.7	22.2	23.9	22.7	22.5	14.0
C	3.1	9.8	8.3	4.2	10.4	10.4	3.7
BN	0.1	6.5	6.1	1.8	4.3	4.4	5.0

^aWe used the finite-temperature correction of +0.577 GPa computed in Ref. [65] for SiO₂.

when added to SCAN, such as from rVV10 [85,88], reinforcing the conclusion of Ref. [65] that adding empirical dispersion for covalent materials is not always pertinent, especially in highly symmetric solids.

B. Transitions involving a low-symmetry phase

For the second group of materials an accurate treatment of correlation at all ranges can be necessary to produce accurate results, though the details of the electronic structure are also important. Similarly to the first group of materials without temperature corrections, SCAN is accurate but overestimates the experimental transition pressure of GaAs while PBE and LDA noticeably underestimate it. The ACFD methods also show analogous trends to the first group with EXX greatly overestimating the transition pressure due to its repulsive nature. With the addition of RPA correlation, the transition pressure drops back down to a reasonable value but still overestimates in comparison to experiment. Adding bRPA correlation from rAPBE at any level of RPA_r again reduces the transition pressure of RPA and comes quite close to experiment. For GaAs, SCAN is actually closer to the bRPA methods than RPA, though all of those methods are within 2 GPa of one another.

For SiO₂, the situation is noticeably different than for the first group of materials or even GaAs. LDA completely fails in this system, yielding an incorrect phase ordering compared to experiment even though the equilibrium volumes are acceptably accurate. PBE serendipitously predicts a reasonably large transition pressure for this system within 2 GPa of experiment, though it systematically overestimates the structural parameters. Our results for these functionals closely match those from previous studies [6,65]. In this material SCAN does not systematically improve upon PBE for the equilibrium energy difference or transition pressure, though the equilibrium volumes are much more accurate compared to experiment. One possible source of difficulty for this family of nonempirical semilocal functionals is strongly polar (almost ionic) bonds in silica from the large difference in electronegativity between Si and O, causing self-interaction errors to more prominently manifest themselves.

Fortunately, the ACFD methods are self-interaction free in the exchange energy, but it is clear from Tables II and III that correlation still makes a huge impact on the results for SiO₂ since EXX overestimates the equilibrium energy difference and transition pressure by nearly a factor of two. As before, RPA correlation tames the wild errors of EXX, but in this case results in an underestimate of the equilibrium energy difference and transition pressure by nearly the same factor that EXX overestimates. Our energy difference and transition pressure for RPA are smaller than those reported by Xiao *et al.* [7], though the general trends compared to experiment are consistent. Reference [7] attributes this failure of RPA to its poor performance for some molecular-like solids where there is less cancellation of errors between dissimilar phases. Looking at the difference between RPA and bRPA results, the root of the RPA error clearly stems from the inaccurate treatment of short-ranged correlation which can be improved through the inclusion of an exchange-correlation kernel correction.

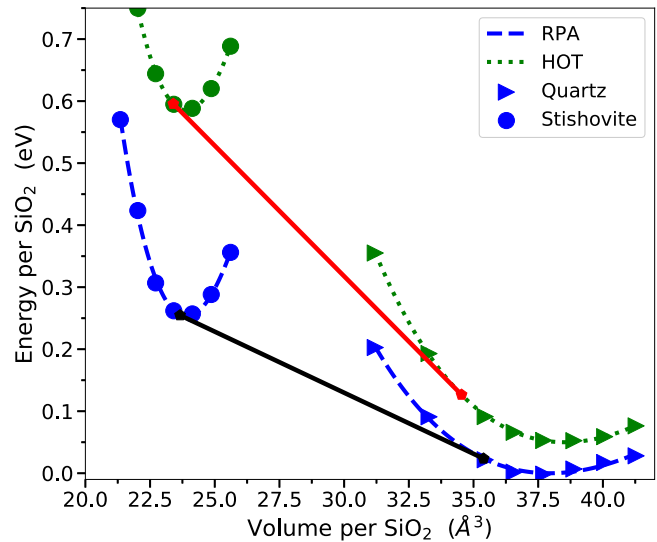


FIG. 4. E - V curve for quartz and stishovite phases of SiO₂ with RPA and bRPA per functional unit. The kernel corrections for SiO₂ increase the equilibrium energy difference of the phases and hence correct the large underestimation of the transition pressure by RPA. The kernel-corrected curves have been rigidly shifted up in energy by 0.05 eV compared to RPA for visual clarity.

The addition of the rAPBE corrections to RPA with any approximation of RPA_r subsequently increases the equilibrium energy difference and transition pressure by raising the energy per SiO₂ of stishovite by approximately 260 meV more than it raises the energy of quartz; see Fig. 4. The resulting theoretical energy difference and transition pressure are increased compared to RPA and are consequently some of the most accurate reported to date for this material, surpassing even the HSE06 screened-hybrid results reported in Ref. [65]. Comparing semilocal and ACFD methods is also unlike with the previous materials since the behavior of the semilocal functionals is erratic at best and RPA struggles due to its inherent limitations, while the bRPA methods continue to deliver high-quality phase transition parameters since they are one-electron SIE free [138] and treat correlation at all ranges of electron-electron interactions. Similar results are expected for other many-body bRPA methods such as SOSEX [31] or AXK [34] since they also tend to be one-electron, but not many-electron SIE free [138,139].

The addition of thermal corrections for GaAs and SiO₂ is also similar to that for the first group in that the thermal corrections typically introduce only a rigid shift in the performance of all the methods. For GaAs the finite-temperature corrections reduce the transition pressures while for SiO₂ they increase the pressure and energy difference mostly due to entropic effects [65,140]. These shifts do not change the relative relationships between functionals or experiment, and are not necessarily crucial for these materials where the energy gap between phases is appreciable.

An essentially rigid shift is also introduced to the results with the addition of an empirical dispersion correction; see the Supplemental Material [108] for numerical results for SiO₂. As reported in Ref. [65], addition of dispersion for SiO₂ reduces the equilibrium volumes and equilibrium energy differences,

though we do find that the magnitude of the shift depends on the damping and functional for which the correction was parametrized. For instance, in Ref. [65] the addition of D2 to TPSS produced a large negative shift in the transition pressure which actually results in a final transition pressure which is slightly negative. For the newer D3 scheme for both PBE and SCAN, the shifts are still 1–3 GPa to smaller pressures, and the zero-damping scheme tends to produce smaller shifts than the Becke-Johnson (BJ) type damping [91]. Adding rVV10 to SCAN also results in shifts similar to D3 with BJ damping.

C. Special cases

The third group of materials is those for which there are some special circumstances that cause unexpected results or for which near degeneracies make it difficult to properly assess semilocal functionals. For Pb, a heavy group IV element, relativistic effects can play an important role in determining the electronic structure. Though the PAW data sets that we have used include scalar relativistic effects for the core and valence electrons [102,104], this may not be enough when full relativistic effects in the valence are also crucial. For the fcc phase of Pb the relativistic treatment of the core electrons is sufficient, since for both semilocal and ACFD methods the performance trends for the structural parameters follow those for the other materials. For the hcp phase, however, the full relativistic effects in the valence are sizable [69] and consequently all of the methods we applied yield large overestimates of the equilibrium volume. The transition pressure predicted for Pb shows a remarkable cancellation of errors considering the gross overestimation of the hcp equilibrium volume. Without temperature corrections, LDA, PBE, and SCAN all underestimate the experimental transition pressure, with PBE yielding a larger transition pressure than the other two. EXX evaluated with PBE orbitals fails spectacularly yet again, yielding roughly triple the experimental value. The addition of correlation from RPA reduces the roughly 20 GPa error of EXX down to about 4 GPa, but is still an overestimate compared to experiment, Table II. The bRPA corrections reduce the transition pressure predicted by RPA by 1–2 GPa, further decreasing the error but still resulting in overestimates of the experimental value. Comparing semilocal and ACFD methods, the former systematically underestimate by a slightly larger margin than the latter overestimate, though the spread in results of both sets of methods is roughly the same.

Though nonrelativistic methods are entirely appropriate for carbon and boron nitride materials, the near degeneracies at 0 K encountered for the cubic and hexagonal phases of these materials complicate predictions of the pressure-induced phase transitions. All of the methods produce reasonably accurate structures for both phases of C and BN, but the predictions for the relative stabilities and transition pressures prove to be challenging for some of the methods. In particular, Table III shows that LDA fails to predict the proper phase ordering for both C and BN, as it did for SiO₂, and so the zero-temperature transition pressures are also inaccurate. PBE and SCAN both overestimate the transition pressure for C and underestimate it for BN, though SCAN is more accurate for C and PBE is more accurate for BN. EXX yields a surprisingly reasonable result for the transition pressure of C, being only about 1.5 GPa larger

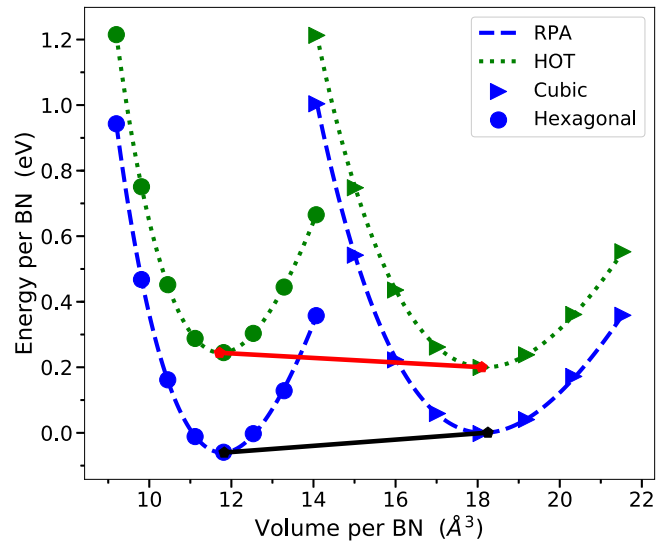


FIG. 5. E - V curve for cubic and hexagonal phases of BN with RPA and RPA with kernel correction per functional unit. Accounting for beyond-RPA correlation through an exchange-correlation kernel for BN changes the sign of the relative energy difference between the phases and hence corrects the errors of RPA. The kernel-corrected curves have been rigidly shifted up in energy by 0.2 eV compared to RPA for visual clarity.

than that predicted by PBE, though it yields a significantly larger transition pressure for BN than the semilocal functionals we tested.

The performance of the correlated methods for C and BN is noticeably different than for the previous materials as well. Earlier RPA calculations indicated nearly degenerate phases for carbon in the diamond and graphite phases [78], and our results also confirm this behavior of the simplest ACFD correlation method. The addition of beyond-RPA correlation, however, increases the energy difference between phases by raising the energy of graphite relative to diamond and yielding transition pressures at zero temperature that are overestimates in comparison to the finite-temperature experiments. We double-checked that this large shift is not unique to the rAPBE kernel by computing the rALDA [100] results, which were indeed very close to the rAPBE results in Tables II and III. Thus without access to other efficient exchange-correlation kernels at this time, it is difficult to understand why these two kernels generate such a large shift in the RPA result for carbon. For BN, however, RPA fails to predict the proper phase ordering akin to LDA; see Fig. 5. The addition of bRPA correlation from rAPBE corrects this deficiency and produces a small positive energy difference and transition pressure between the cubic and hexagonal phases. Since BN involves heteronuclear bonds, an accurate treatment of short-ranged correlation is likely needed to obtain good results, which we are able to achieve with the rAPBE kernel at any level of RPA renormalization, whereas for carbon the natural cancellation of errors of RPA results in an accurate result. For these two materials it is difficult to select one among the semilocals or ACFD methods that is most accurate since the errors are of similar magnitudes though with differing signs.

The addition of thermal corrections for Pb, C, and BN tends to unilaterally destabilize the high-pressure phase resulting in a positive shift to the zero-temperature transition pressures. For Pb, which is typically considered a very soft metal, the thermal corrections from PBE unilaterally result in overestimates of the finite-temperature transition pressure for all methods, though the spread in the results is noticeably decreased. Thus it is clear that the zero-temperature results benefit from cancellation of opposing effects generated by the stabilization due to relativity and destabilization due to phonons in the hcp phase. For C and BN at finite temperature, RPA is quite close to experiment for the former but not the latter, while the bRPA methods are more accurate for BN than for C.

The addition of empirical dispersion was also explored for Pb and BN and is reported in the Supplemental Material [108]. For Pb, adding the dispersion corrections also reduces the transition pressures. For PBE+D3 the reduction is close to 1.5 GPa, but for PBE+D2 it is closer to 4.5 GPa. Adding the D3 correction to SCAN hardly changes the SCAN result; however addition of rVV10 results in a 2 GPa reduction of the transition pressure bringing it close to that predicted by PBE+D2. Though addition of the dispersion corrections to Pb yields a reduction in the transition pressure similarly to Zr, the addition of thermal corrections increases the transition pressure of Pb whereas it reduces the transition pressure of Zr [65]. Also the magnitude of the shift due to thermal corrections in Pb is much higher than that of Zr because of the presence of soft phonon modes.

For BN the effects of empirical dispersion are similar to the other materials, resulting in reduction of the equilibrium volumes and the transition pressures. The shifts induced by the D3 correction tend to be smaller than those of D2 and rVV10 for PBE and SCAN, respectively. In fact, the addition of D2 decreases the energy difference between phases so much that for PBE it changes the phase ordering, being now similar to RPA and resulting in a negative transition pressure. SCAN+rVV10 ultimately gives a value very close to that of bRPA methods for BN, though SCAN+D3 is also within 1 GPa as well.

Figure 6 summarizes the finite-temperature results at 300 K and illustrates the relative performance of the selected methods with respect to experiment. SCAN tends to be the most accurate semilocal functional and yields results in good agreement with RPA. Overall, the thermally corrected bRPA methods yield consistent accuracy for all of materials. The small differences between RPA methods also indicate that the details of the bRPA method are not crucial, just that one must account for beyond-RPA correlation in a nonperturbative way as to avoid divergences for small-gap systems.

V. DISCUSSION AND CONCLUSIONS

We evaluated the performance of LDA, PBE, SCAN, RPA, and beyond-RPA methods from RPA renormalization using the rAPBE exchange-like kernel in a comparative study for the determination of structural properties and transition parameters of different phases. Both the zero-temperature electronic structure calculations of the ground state and the finite-temperature predictions with thermal corrections from the phonons were compared with experimental results. For materials with two

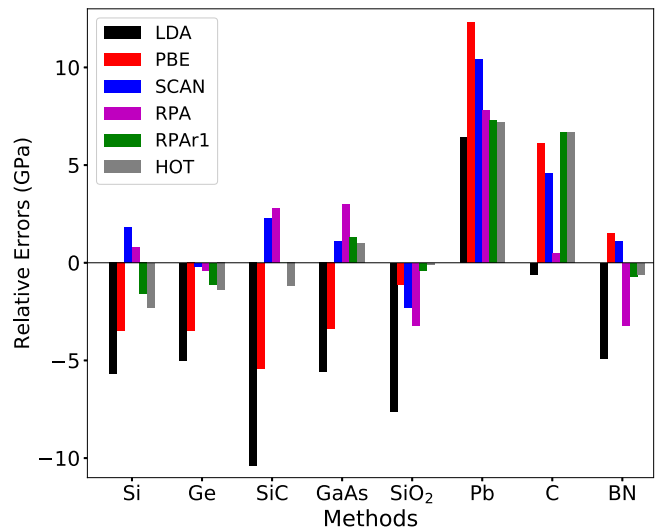


FIG. 6. Relative errors (GPa) compared to experiment of the transition pressures at room temperature predicted by each method for each system. As explained in the text, the RPAr1 value is used as the reference value for SiC instead of the experimental result.

high-symmetry phases and an appreciable energy difference between phases, semilocal density functionals are usefully accurate and the improvements from the ACFD methods are not substantial. For materials with dissimilar phases, semilocal functionals can struggle to produce systematic results from one functional to the next, especially in cases such as SiO₂ where self-interaction error can play an important role. The ACFD methods tend to improve upon the semilocal functionals for GaAs, though the inherent limitations of RPA can still result in poor results for molecular-like systems such as silica. For materials which require special consideration to understand their behavior, the ACFD methods tend to produce the most consistent results, though SCAN can also be a practical choice in these materials for compromising between speed and accuracy.

In general, methods such as RPAr1 evaluated with the rAPBE kernel should yield the most consistent results across all types of materials. Based on a self-interaction free exchange energy, bRPA methods accurately treat long-range interactions because they are based upon RPA correlation, as well as being accurate for short-ranged interactions due to the explicit inclusion of an exchange-correlation kernel. Since all length scales of the electron-electron interaction are accounted for systematically one can expect the results produced by bRPA methods to be intentionally accurate and not rely on cancellation of errors as is the case for semilocal functionals. Furthermore, higher orders of RPA do not make a large contribution to the phase transition parameters since the difference between the HOT method and RPAr1 tends to be negligible. Since SCAN also accounts for different ranges of electronic interactions, it delivers the highest quality semilocal results. Through its meta-GGA form SCAN captures the usual short-ranged exchange and correlation effects of earlier semilocal functionals. Furthermore, it includes medium-range van der Waals interactions that are missing in, e.g., LDA or PBE. SCAN still benefits somewhat from residual self-interaction

errors and a lack of long-range dispersion which tend to offset each other, since the former is repulsive and the latter attractive. Therefore we can recommend SCAN as a general method to represent semilocal functionals when exploring new materials or phase transitions, and that the bRPA methods can be used as quality control for both energy differences and transition pressures whenever accurate experimental results are unavailable.

Thermal corrections and empirical dispersion were also explored as additional corrections to all methods and the semilocal functionals, respectively. The former can either stabilize or destabilize the high-pressure phase, but in general the shifts introduced by phononic corrections are smaller than the differences in performance for the various methods. For soft materials or those with near degeneracies, including the thermal corrections can be crucial to obtain consistent results with experiment. The addition of dispersion, on the other hand, can often lead to worse results than from the pure semilocal functionals since it tends to shrink equilibrium volumes and reduce the equilibrium energy difference between different phases of a material. In this way, the additional attraction provided by empirical dispersion is not offset by any repulsive contributions (such as from self-interaction corrections) and so must be used with caution when studying bulk materials [65].

One point not discussed explicitly thus far is that the difference in behavior of exchange and correlation in semilocal functionals and ACFD methods is striking. For the former, the

exchange potential and energy often comprise the majority of the binding described by density functional approximations, and the addition of the correlation potential and energy often induce only a (relatively) small shift from the exchange-only results. For the ACFD, however, non-self-consistent EXX typically underbinds by a considerable degree resulting in wildly inaccurate results. Thus the addition of correlation leads to very large shifts in the exchange-only results, in direct contrast to semilocal correlation. This difference in behavior is directly linked to the nonlocal nature of the EXX, and even though the exchange-only starting point is often nowhere close to experiment, the nonlocal correlation from the ACFD corrects this deficiency and yields the missing binding needed to produce accurate results. Thus we find the ACFD approach to be vital in the validation of semilocal results and recommend its use in materials where experimental results cannot be straightforwardly compared to other approximate electronic structure calculations.

ACKNOWLEDGMENTS

J.E.B. and A.R. acknowledge National Science Foundation for providing the financial support under Grant No. DMR-1553022 to finish this project. This work was also supported in part by the National Science Foundation through major research instrumentation Grant No. CNS-09-58854. Figures were created using MATPLOTLIB [142].

-
- [1] P. G. Radaelli, G. Iannone, M. Marezio, H. Y. Hwang, S. W. Cheong, J. D. Jorgensen, and D. N. Argyriou, *Phys. Rev. B* **56**, 8265 (1997).
 - [2] V. K. Vlasko-Vlasov, Y. K. Lin, D. J. Miller, U. Welp, G. W. Crabtree, and V. I. Nikitenko, *Phys. Rev. Lett.* **84**, 2239 (2000).
 - [3] A. Kato, M. Nishigaki, N. Mamedov, M. Yamazaki, S. Abdullayeva, E. Kerimova, H. Uchiki, and S. Iida, *J. Phys. Chem. Solids* **64**, 1713 (2003).
 - [4] Y. Kang, S. Najmaei, Z. Liu, Y. Bao, Y. Wang, X. Zhu, N. J. Halas, P. Nordlander, P. M. Ajayan, J. Lou *et al.*, *Adv. Mater.* **26**, 6467 (2014).
 - [5] J. P. Perdew, J. A. Chevary, S. H. Vosko, K. A. Jackson, M. R. Pederson, D. J. Singh, and C. Fiolhais, *Phys. Rev. B* **46**, 6671 (1992).
 - [6] A. Mujica, A. Rubio, A. Munoz, and R. Needs, *Rev. Mod. Phys.* **75**, 863 (2003).
 - [7] B. Xiao, J. Sun, A. Ruzsinszky, J. Feng, and J. P. Perdew, *Phys. Rev. B* **86**, 094109 (2012).
 - [8] Y. Zhang and W. Yang, *J. Chem. Phys.* **109**, 2604 (1998).
 - [9] J. P. Perdew and A. Zunger, *Phys. Rev. B* **23**, 5048 (1981).
 - [10] P. Mori-Sánchez, A. J. Cohen, and W. Yang, *J. Chem. Phys.* **125**, 201102 (2006).
 - [11] T. Schmidt and S. Kümmel, *Computation* **4**, 33 (2016).
 - [12] A. Heßelmann and A. Görling, *Mol. Phys.* **109**, 2473 (2011).
 - [13] H. Eshuis, J. E. Bates, and F. Furche, *Theor. Chem. Acc.* **131**, 1084 (2012).
 - [14] X. Ren, P. Rinke, C. Joas, and M. Scheffler, *J. Mater. Sci.* **47**, 7447 (2012).
 - [15] J. Harl and G. Kresse, *Phys. Rev. B* **77**, 045136 (2008).
 - [16] L. Schimka, J. Harl, A. Stroppa, A. Grüneis, M. Marsman, F. Mittendorfer, and G. Kresse, *Nat. Mater.* **9**, 741 (2010).
 - [17] S. Lebègue, J. Harl, T. Gould, J. G. Ángyán, G. Kresse, and J. F. Dobson, *Phys. Rev. Lett.* **105**, 196401 (2010).
 - [18] H. Eshuis and F. Furche, *J. Phys. Chem. Lett.* **2**, 983 (2011).
 - [19] T. Björkman, A. Gulans, A. V. Krasheninnikov, and R. M. Nieminen, *Phys. Rev. Lett.* **108**, 235502 (2012).
 - [20] J. Harl, L. Schimka, and G. Kresse, *Phys. Rev. B* **81**, 115126 (2010).
 - [21] H. Peng and S. Lany, *Phys. Rev. B* **87**, 174113 (2013).
 - [22] A. M. Burow, J. E. Bates, F. Furche, and H. Eshuis, *J. Chem. Theory Comput.* **10**, 180 (2014).
 - [23] T. Olsen and K. S. Thygesen, *Phys. Rev. B* **87**, 075111 (2013).
 - [24] C. E. Patrick and K. S. Thygesen, *J. Chem. Phys.* **143**, 102802 (2015).
 - [25] L. Schimka, R. Gaudoin, J. Klimeš, M. Marsman, and G. Kresse, *Phys. Rev. B* **87**, 214102 (2013).
 - [26] C. E. Patrick and K. S. Thygesen, *Phys. Rev. B* **93**, 035133 (2016).
 - [27] F. Furche, *Phys. Rev. B* **64**, 195120 (2001).
 - [28] Z. Yan, J. P. Perdew, and S. Kurth, *Phys. Rev. B* **61**, 16430 (2000).
 - [29] A. Ruzsinszky, J. P. Perdew, and G. I. Csonka, *J. Chem. Theory Comput.* **6**, 127 (2010).
 - [30] J. E. Bates, S. Laricchia, and A. Ruzsinszky, *Phys. Rev. B* **93**, 045119 (2016).
 - [31] A. Grüneis, M. Marsman, J. Harl, L. Schimka, and G. Kresse, *J. Chem. Phys.* **131**, 154115 (2009).

- [32] G. Jansen, R.-F. Liu, and J. G. Ángyán, *J. Chem. Phys.* **133**, 154106 (2010).
- [33] T. Olsen and K. S. Thygesen, *Phys. Rev. B* **86**, 081103 (2012).
- [34] J. E. Bates and F. Furche, *J. Chem. Phys.* **139**, 171103 (2013).
- [35] T. Olsen and K. S. Thygesen, *Phys. Rev. Lett.* **112**, 203001 (2014).
- [36] M. T. Yin and M. L. Cohen, *Phys. Rev. B* **26**, 5668 (1982).
- [37] A. Dal Corso, A. Pasquarello, A. Baldereschi, and R. Car, *Phys. Rev. B* **53**, 1180 (1996).
- [38] N. Moll, M. Bockstedte, M. Fuchs, E. Pehlke, and M. Scheffler, *Phys. Rev. B* **52**, 2550 (1995).
- [39] A. S. Kashyap, C.-P. Chen, R. Ghandi, A. Patil, E. Andarawis, L. Yin, D. Shaddock, P. Sandvik, K. Fang, Z. Shen *et al.*, in *IEEE Workshop on Wide Bandgap Power Devices and Applications (WiPDA), 2013* (IEEE, Columbus, OH, 2000), pp. 60–63.
- [40] K. Schwetz, in *Handbook of Ceramic Hard Materials*, edited by R. Riedel (Wiley-VCH Verlag GmbH, Weinheim, 2013), pp. 683–748.
- [41] K. Karch, P. Pavone, W. Windl, O. Schütt, and D. Strauch, *Phys. Rev. B* **50**, 17054 (1994).
- [42] K. J. Chang and M. L. Cohen, *Phys. Rev. B* **35**, 8196 (1987).
- [43] M. Yoshida, A. Onodera, M. Ueno, K. Takemura, and O. Shimomura, *Phys. Rev. B* **48**, 10587 (1993).
- [44] M. Catti, *Phys. Rev. Lett.* **87**, 035504 (2001).
- [45] M. S. Miao and W. R. L. Lambrecht, *Phys. Rev. B* **68**, 092103 (2003).
- [46] K. Karch, F. Bechstedt, P. Pavone, and D. Strauch, *Phys. Rev. B* **53**, 13400 (1996).
- [47] M. Durandurdu, *Phys. Rev. B* **75**, 235204 (2007).
- [48] B. J. Baliga, *IEEE Electron Device Lett.* **10**, 455 (1989).
- [49] J. Blakemore, *J. Appl. Phys.* **53**, R123 (1982).
- [50] G. B. Bachelet and N. E. Christensen, *Phys. Rev. B* **31**, 879 (1985).
- [51] D. Eastman, W. Grobman, J. Freeouf, and M. Erbudak, *Phys. Rev. B* **9**, 3473 (1974).
- [52] T. W. Crowe, R. J. Mattauch, H. Roser, W. L. Bishop, W. C. Peatman, and X. Liu, *Proc. IEEE* **80**, 1827 (1992).
- [53] W. R. Curtice, *IEEE Trans. Microw. Theory Tech.* **28**, 448 (1980).
- [54] R. Van Tuyl, V. Kumar, D. D’Avanzo, T. Taylor, V. Peterson, D. Hornbuckle, R. Fisher, and D. Estreich, *IEEE Trans. Microw. Theory Tech.* **30**, 935 (1982).
- [55] A. Gobat, M. Lamorte, and G. McIver, *IEEE Trans. Mil. Electron.* **1051**, 20 (1962).
- [56] S. Minomura and H. Drickamer, *J. Phys. Chem. Solids* **23**, 451 (1962).
- [57] S. T. Weir, Y. K. Vohra, C. A. Vanderborgh, and A. L. Ruoff, *Phys. Rev. B* **39**, 1280 (1989).
- [58] R. J. Nelmes and M. I. McMahon, *Phys. Rev. Lett.* **74**, 106 (1995).
- [59] J. M. Besson, J. P. Itié, A. Polian, G. Weill, J. L. Mansot, and J. Gonzalez, *Phys. Rev. B* **44**, 4214 (1991).
- [60] P. Atkins, T. Overton, J. Rourke, M. Weller, and F. Armstrong, *Shriver & Atkins’ Inorganic Chemistry*, 5th ed. (Oxford University Press, 2010).
- [61] B. Holm and R. Ahuja, *J. Chem. Phys.* **111**, 2071 (1999).
- [62] N. Choudhury and S. L. Chaplot, *Phys. Rev. B* **73**, 094304 (2006).
- [63] B. B. Karki, M. C. Warren, L. Stixrude, G. J. Ackland, and J. Crain, *Phys. Rev. B* **55**, 3465 (1997).
- [64] J. P. Perdew, K. Burke, and M. Ernzerhof, *Phys. Rev. Lett.* **77**, 3865 (1996).
- [65] B. Xiao, J. Sun, A. Ruzsinszky, J. Feng, R. Haunschild, G. E. Scuseria, and J. P. Perdew, *Phys. Rev. B* **88**, 184103 (2013).
- [66] C. A. Vanderborgh, Y. K. Vohra, H. Xia, and A. L. Ruoff, *Phys. Rev. B* **41**, 7338 (1990).
- [67] H. Mao, Y. Wu, J. Shu, J. Hu, R. Hemley, and D. Cox, *Solid State Commun.* **74**, 1027 (1990).
- [68] A. Y. Liu, A. Garcia, M. L. Cohen, B. K. Godwal, and R. Jeanloz, *Phys. Rev. B* **43**, 1795 (1991).
- [69] A. Hermann, J. Furthmüller, H. W. Gäggeler, and P. Schwerdtfeger, *Phys. Rev. B* **82**, 155116 (2010).
- [70] L. Vel, G. Demazeau, and J. Etourneau, *Mater. Sci. Eng. B* **10**, 149 (1991).
- [71] R. F. Davis, *Proc. IEEE* **79**, 702 (1991).
- [72] R. M. Wentzcovitch, S. Fahy, M. L. Cohen, and S. G. Louie, *Phys. Rev. B* **38**, 6191 (1988).
- [73] J. Furthmüller, J. Hafner, and G. Kresse, *Phys. Rev. B* **50**, 15606 (1994).
- [74] V. L. Solozhenko, V. Z. Turkevich, and W. B. Holzapfel, *J. Phys. Chem. B* **103**, 2903 (1999).
- [75] K. Albe, *Phys. Rev. B* **55**, 6203 (1997).
- [76] G. Kern, G. Kresse, and J. Hafner, *Phys. Rev. B* **59**, 8551 (1999).
- [77] F. Bundy, W. Bassett, M. Weathers, R. Hemley, H. Mao, and A. Goncharov, *Carbon* **34**, 141 (1996).
- [78] J. Harl and G. Kresse, *Phys. Rev. Lett.* **103**, 056401 (2009).
- [79] C. Mailhiot and A. K. McMahan, *Phys. Rev. B* **44**, 11578 (1991).
- [80] Z.-H. Cui, F. Wu, and H. Jiang, *Phys. Chem. Chem. Phys.* **18**, 29914 (2016).
- [81] S. R. Whittleton, A. Otero-de-la Roza, and E. R. Johnson, *J. Chem. Theory Comput.* **13**, 5332 (2017).
- [82] J. P. Perdew, K. Schmidt, V. Van Doren, C. Van Alsenoy, and P. Geerlings, in *Density Functional Theory and Its Application to Materials*, AIP Conference Proceedings Vol. 577 (AIP, Antwerp, Belgium, 2001), pp. 1–20.
- [83] U. von Barth and L. Hedin, *J. Phys. C* **5**, 1629 (1972).
- [84] J. Sun, A. Ruzsinszky, and J. P. Perdew, *Phys. Rev. Lett.* **115**, 036402 (2015).
- [85] H. Peng, Z.-H. Yang, J. P. Perdew, and J. Sun, *Phys. Rev. X* **6**, 041005 (2016).
- [86] J. G. Brandenburg, J. E. Bates, J. Sun, and J. P. Perdew, *Phys. Rev. B* **94**, 115144 (2016).
- [87] O. A. Vydrov and T. Van Voorhis, *J. Chem. Phys.* **133**, 244103 (2010).
- [88] R. Sabatini, T. Gorni, and S. de Gironcoli, *Phys. Rev. B* **87**, 041108 (2013).
- [89] S. Grimme, *J. Comput. Chem.* **27**, 1787 (2006).
- [90] S. Grimme, J. Antony, S. Ehrlich, and H. Krieg, *J. Chem. Phys.* **132**, 154104 (2010).
- [91] S. Grimme, S. Ehrlich, and L. Goerigk, *J. Comput. Chem.* **32**, 1456 (2011).
- [92] D. C. Langreth and J. P. Perdew, *Solid State Commun.* **17**, 1425 (1975).
- [93] M. Lein, E. K. U. Gross, and J. P. Perdew, *Phys. Rev. B* **61**, 13431 (2000).

- [94] F. Furche and T. Van Voorhis, *J. Chem. Phys.* **122**, 164106 (2005).
- [95] J. E. Bates, P. D. Mezei, G. I. Csonka, J. Sun, and A. Ruzsinszky, *J. Chem. Theory Comput.* **13**, 100 (2017).
- [96] J. E. Bates, J. Sensenig, and A. Ruzsinszky, *Phys. Rev. B* **95**, 195158 (2017).
- [97] J. E. Bates, N. Sengupta, J. Sensenig, and A. Ruzsinszky, *J. Chem. Theory Comput.* **14**, 2979 (2018).
- [98] D. C. Langreth and J. P. Perdew, *Phys. Rev. B* **15**, 2884 (1977).
- [99] N. Colonna, M. Hellgren, and S. de Gironcoli, *Phys. Rev. B* **90**, 125150 (2014).
- [100] T. Olsen and K. S. Thygesen, *Phys. Rev. B* **88**, 115131 (2013).
- [101] J. J. Mortensen, L. B. Hansen, and K. W. Jacobsen, *Phys. Rev. B* **71**, 035109 (2005).
- [102] J. Enkovaara, C. Rostgaard, J. J. Mortensen, J. Chen, M. Dułak, L. Ferrighi, J. Gavnholt, C. Glinsvad, V. Haikola, H. A. Hansen, H. H. Kristoffersen, M. Kuisma, A. H. Larsen, L. Lehtovaara, M. Ljungberg, O. Lopez-Acevedo, P. G. Moses, J. Ojanen, T. Olsen, V. Petzold, N. A. Romero, J. Stausholm-Møller, M. Strange, G. A. Tritsaridis, M. Vanin, M. Walter, B. Hammer, H. Häkkinen, G. K. H. Madsen, R. M. Nieminen, J. K. Nørskov, M. Puska, T. T. Rantala, J. Schiøtz, K. S. Thygesen, and K. W. Jacobsen, *J. Phys.: Condens. Matter* **22**, 253202 (2010).
- [103] S. R. Bahn and K. W. Jacobsen, *Comput. Sci. Eng.* **4**, 56 (2002).
- [104] P. E. Blöchl, *Phys. Rev. B* **50**, 17953 (1994).
- [105] H. J. Monkhorst and J. D. Pack, *Phys. Rev. B* **13**, 5188 (1976).
- [106] P. E. Trevisanutto, A. Terentjevs, L. A. Constantin, V. Olevano, and F. D. Sala, *Phys. Rev. B* **87**, 205143 (2013).
- [107] G. Kresse and J. Hafner, *Phys. Rev. B* **47**, 558 (1993).
- [108] See Supplemental Material at <http://link.aps.org/supplemental/10.1103/PhysRevB.97.235136> for a compressed file containing raw data, as well as a pdf describing the contents of the compressed file, some computational details, and results not discussed in the main paper.
- [109] S. Baroni, S. De Gironcoli, A. Dal Corso, and P. Giannozzi, *Rev. Mod. Phys.* **73**, 515 (2001).
- [110] X. Gonze and C. Lee, *Phys. Rev. B* **55**, 10355 (1997).
- [111] G. Kresse and D. Joubert, *Phys. Rev. B* **59**, 1758 (1999).
- [112] A. Landerville, M. Conroy, M. Budzevich, Y. Lin, C. White, and I. Olevnik, *Appl. Phys. Lett.* **97**, 251908 (2010).
- [113] R. M. Wentzcovitch, G. Y. Yonggang, and Z. Wu, *Rev. Mineral. Geochem.* **71**, 59 (2010).
- [114] B. B. Karki and R. M. Wentzcovitch, *J. Geophys. Res.* **B 107**, 2267 (2002).
- [115] R. Wentzcovitch, L. Stixrude, B. Karki, and B. Kiefer, *Geophys. Res. Lett.* **31**, L10611 (2004).
- [116] M. L. Marcondes, R. M. Wentzcovitch, and L. V. Assali, *Solid State Commun.* **273**, 11 (2017).
- [117] F. D. Murnaghan, *Proc. Natl. Acad. Sci. USA* **30**, 244 (1944).
- [118] F. Birch, *Phys. Rev.* **71**, 809 (1947).
- [119] N. Mounet and N. Marzari, *Phys. Rev. B* **71**, 205214 (2005).
- [120] J. D. Althoff, P. B. Allen, R. M. Wentzcovitch, and J. A. Moriarty, *Phys. Rev. B* **48**, 13253 (1993).
- [121] I. Hamdi and N. Meskini, *Physica B: Condensed Matter* **405**, 2785 (2010).
- [122] P. Pavone, S. Baroni, and S. de Gironcoli, *Phys. Rev. B* **57**, 10421 (1998).
- [123] K. Gaál-Nagy, A. Bauer, M. Schmitt, K. Karch, P. Pavone, and D. Strauch, *Phys. Status Solidi B* **211**, 275 (1999).
- [124] B. Ramberger, T. Schäfer, and G. Kresse, *Phys. Rev. Lett.* **118**, 106403 (2017).
- [125] R. Gaudoin and W. M. C. Foulkes, *Phys. Rev. B* **66**, 052104 (2002).
- [126] G. I. Csonka, J. P. Perdew, A. Ruzsinszky, P. H. T. Philipsen, S. Lebègue, J. Paier, O. A. Vydrov, and J. G. Ángyán, *Phys. Rev. B* **79**, 155107 (2009).
- [127] P. Haas, F. Tran, and P. Blaha, *Phys. Rev. B* **79**, 085104 (2009).
- [128] A. B. Alchagirov, J. P. Perdew, J. C. Boettger, R. C. Albers, and C. Fiolhais, *Phys. Rev. B* **63**, 224115 (2001).
- [129] B. H. Cheong and K. J. Chang, *Phys. Rev. B* **44**, 4103 (1991).
- [130] J. C. Boettger and S. B. Trickey, *Phys. Rev. B* **53**, 3007 (1996).
- [131] N. E. Christensen and M. Methfessel, *Phys. Rev. B* **48**, 5797 (1993).
- [132] P. Vinet, J. H. Rose, J. Ferrante, and J. R. Smith, *J. Phys.: Condens. Matter* **1**, 1941 (1989).
- [133] M. I. McMahon, R. J. Nelmes, N. G. Wright, and D. R. Allan, *Phys. Rev. B* **50**, 739 (1994).
- [134] A. Jain, S. P. Ong, G. Hautier, W. Chen, W. D. Richards, S. Dacek, S. Cholia, D. Gunter, D. Skinner, G. Ceder, and K. A. Persson, *APL Mater.* **1**, 011002 (2013).
- [135] D. Rappoport, N. R. M. Crawford, F. Furche, and K. Burke, Approximate density functionals: Which should I choose? in *Encyclopedia of Inorganic Chemistry* (John Wiley & Sons Ltd., New York, 2006).
- [136] J. Sun, R. C. Remsing, Y. Zhang, Z. Sun, A. Ruzsinszky, H. Peng, Z. Yang, A. Paul, U. Waghmare, X. Wu *et al.*, *Nat. Chem.* **8**, 831 (2016).
- [137] C. Shahi, J. Sun, and J. P. Perdew, *Phys. Rev. B* **97**, 094111 (2018).
- [138] A. Ruzsinszky, J. P. Perdew, G. I. Csonka, O. A. Vydrov, and G. E. Scuseria, *J. Chem. Phys.* **126**, 104102 (2007).
- [139] T. M. Henderson and G. E. Scuseria, *Mol. Phys.* **108**, 2511 (2010).
- [140] C. Lee and X. Gonze, *Phys. Rev. B* **51**, 8610 (1995).
- [141] D. R. Hamann, *Phys. Rev. Lett.* **76**, 660 (1996).
- [142] J. D. Hunter, *Comput. Sci. Eng.* **9**, 90 (2007).